

# Experimental Decoding Scrambled Quantum Information from the Future

Yi-Te Huang,<sup>1,2,3,4</sup> Siang-Wei Huang,<sup>1,2</sup> Jhen-Dong Lin,<sup>1,2</sup> Adam Miranowicz,<sup>3,4,5</sup>  
Neill Lambert,<sup>3,4</sup> Guang-Yin Chen,<sup>6</sup> Franco Nori,<sup>3,4,7</sup> and Yueh-Nan Chen<sup>1,2,8,\*</sup>

<sup>1</sup>*Department of Physics, National Cheng Kung University, Tainan 701401, Taiwan*

<sup>2</sup>*Center for Quantum Frontiers of Research and Technology (QFort), Tainan 701401, Taiwan*

<sup>3</sup>*RIKEN Center for Quantum Computing, RIKEN, Wakoshi, Saitama 351-0198, Japan*

<sup>4</sup>*Theoretical Quantum Physics Laboratory, Cluster for Pioneering Research, RIKEN, Wakoshi, Saitama 351-0198, Japan*

<sup>5</sup>*Institute of Spintronics and Quantum Information, Faculty of Physics and Astronomy,  
Adam Mickiewicz University, 61-614 Poznań, Poland*

<sup>6</sup>*Department of Physics, National Chung Hsing University, Taichung 402202, Taiwan*

<sup>7</sup>*Physics Department, The University of Michigan, Ann Arbor, Michigan 48109-1040, USA.*

<sup>8</sup>*Physics Division, National Center for Theoretical Sciences, Taipei 106319, Taiwan*

Quantum information scrambling describes the rapid spread of initially localized information across an entire quantum many-body system through entanglement generation. Once scrambled, the original local information becomes encoded globally, inaccessible from any single subsystem. In this work, we introduce a protocol that enables information scrambling into the past, allowing decoding even before the original information is generated. This protocol is achieved by simulating a closed timelike curve—a theoretical construct in which particles can traverse backward in time—using probabilistic methods. Remarkably, we find that stronger scrambling dynamics enhance the fidelity of the decoding process. We further present a quantum circuit design and experimentally implement our protocol on cloud-based Quantinuum and IBM quantum computers. Our approach illuminates a unique quantum task: retrieving information encoded in the future without altering the past.

## I. INTRODUCTION

Quantum information scrambling (QIS) arises from strong interactions in a many-body system [1–3]. Such dynamics rapidly correlates local information and generates many-body entanglement across all possible degrees of freedom within the global system [3–15]. This delocalization process in many-body physics is typically characterized by the decay of the out-of-time-order correlator (OTOC) [1, 2] and has sparked growing interest in various fields, such as quantum chaos [14–24], black hole thermalization and information problems [25–35], quantum collision models [36–38], quantum computing and error correction [39–41].

Local information can be encoded into a global system by utilizing QIS. In a scrambled system, the information becomes dispersed and inaccessible via local measurements due to many-body entanglement. The robustness of recovering the original quantum information depends on the strength and structure of this entanglement [39, 42]. Remarkably, it is possible to recover the information even when parts of the system are damaged or lost. For instance, if the scrambled state is damaged by a local measurement but this damage does not affect the useful information encoded in the entanglement correlations, one can still recover the original information [40, 42].

Another example is when a quantum state is thrown into a black hole, characterized by strong scrambling dynamics, and the information is believed to irretrievably

disappear once it crosses the event horizon [25]. However, Ref. [25] proposed a thought experiment suggesting that it might be possible to probabilistically reconstruct the lost information from several emitted Hawking radiation photons from the black hole through a suitable decoding process. An efficient decoding protocol for this thought experiment was proposed by Yoshida and Kitaev [43], with some extended scenarios [44–46] experimentally demonstrated [47–50]. Yoshida and Kitaev’s probabilistic decoding protocol can also be considered postselected quantum teleportation. The preparation of Einstein-Podolsky-Rosen (EPR) pairs and the corresponding postselection of the measurement outcomes are necessary for the original state (information) to be successfully teleported (decoded) in their protocol.

Recently, the concept of postselected quantum teleportation has led to a unique perspective on the nature of causality and time in quantum mechanics, known as the postselected closed timelike curve (PCTC) [51–53]. A closed timelike curve (CTC) is a hypothetical concept in general relativity that describes a worldline in spacetime looping back on itself, allowing a particle to return to and interact with its own past [54, 55]. This idea suggests the possibility of time travel and may raise some paradoxes [56]. A well-known illustration of time travel paradoxes is the grandfather paradox: a time traveler goes back in time and kills his or her grandfather before the grandfather has any children, effectively preventing her own birth. This kind of logical inconsistency has led to scientific debates about the existence of CTCs [57–64].

PCTCs enable a specific formulation that combines CTCs with quantum mechanics based on quantum teleportation and postselection [51–53]. The scenario begins with the preparation of a bipartite maximally en-

\* yuehnan@mail.ncku.edu.tw

tangled state and concludes with a projective measurement on the same state. The postselection of specific outcomes introduces nonlinear effects into quantum systems. These nonlinearities are crucial for avoiding contradictions, thereby obeying the Novikov self-consistency principle [57]: the events that could cause paradoxes or changes to the past have zero probability. That is, only logically self-consistent events can occur in a PCTC with conditional probabilities, which is also considered the success probability of time travel. For instance, the grandfather paradox can be resolved in a PCTC [52]. The theory of PCTCs offers a valuable formulation to bridge quantum mechanics and general relativity, contributing to the development of quantum theories of gravity [65–67]. Such a formulation can also be applied to quantum information processing [68–71], and benefit some metrological tasks [72, 73].

In this work, we utilize the concept of PCTCs and propose a protocol to transmit scrambled (encrypted) quantum information into the past. Remarkably, we show that *this encrypted message can be decoded even before the original information is generated*. The protocol is quantified by the fidelity between the original state prepared in the future and the decoded state in the past. We show that the decoding fidelity depends on the success probability of time travel through a PCTC. Nevertheless, this success probability depends on the strength of QIS, characterized by the decay of the average value of the OTOC. Therefore, sufficiently strong scrambling dynamics guarantees that the original information to be perfectly decoded (with unity fidelity). Furthermore, we demonstrate our decoding protocol using a four-qubit quantum circuit and then implement it on both Quantinuum [74] and IBM quantum (IBMQ) [75, 76] processors. We compare two different scrambling dynamics to highlight the critical role that QIS plays in our protocol.

The rest of the paper is organized as follows. In Sec. II, we introduce the decoding protocol. In Sec. III, we analyze the decay of the OTOC to characterize QIS and explore its connection to PCTCs within our decoding protocol. Section IV presents the experimental demonstration of the protocol on the Quantinuum and IBMQ processors. Finally, we draw our conclusions in Sec. V.

## II. DECODING PROTOCOL

We introduce a protocol for recovering scrambled information from the future, as illustrated schematically in Fig. 1. Our protocol includes three main steps: (1) encoding quantum information using QIS, (2) time-travel part of the encoded information into the past via a PCTC, and (3) decoding the original information.

We begin with Alice (A), who prepares an arbitrary pure quantum state  $|\psi\rangle$  with Hilbert space dimension  $d_A$  at time  $T_1$ . As time progresses from  $T_1$  to  $T_2$ , system A interacts with a chronology-respecting many-body system H, and the global evolution of this interaction

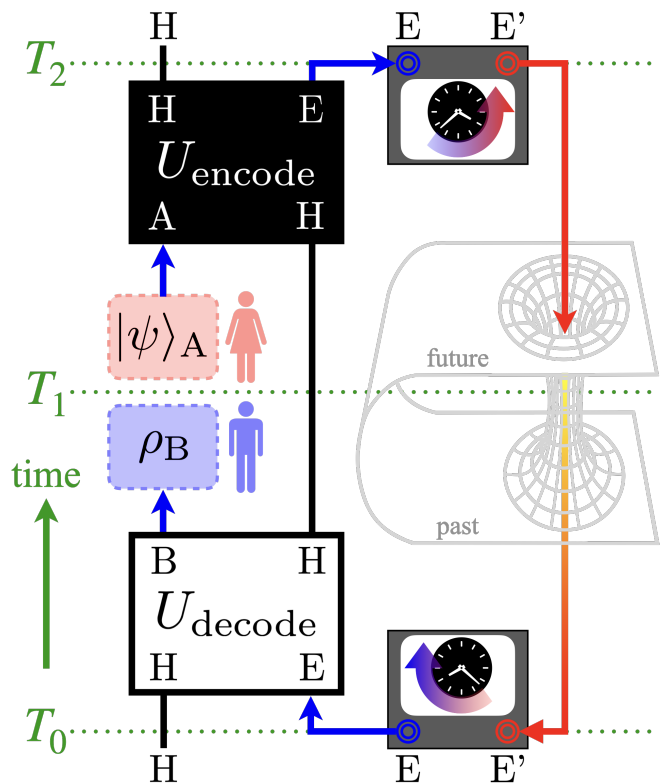


FIG. 1. Schematic illustration of the decoding protocol. The black solid lines depict the timeline of the many-body system H going forwards. The blue (red) arrows depict the timeline of a portion of the encoded information E (E') going forwards (backwards). Starting at time  $T_1$ , Alice (A) sends the information  $|\psi\rangle$  into the scrambling unitary operator (scrambler)  $U_{\text{encode}} = U_{AH \rightarrow HE}$ , encoding the information in the joint system HE at  $T_2$ . By projecting the state of joint system EE' into an EPR state, the temporal direction for E is reversed, causing it to travel backward in time from  $T_2$  to  $T_0$ . Because the state of system E and E' are initialized as an EPR state at  $T_0$ , the temporal direction for E' is reversed again. The decoding unitary operator  $U_{\text{decode}} = U_{HE \rightarrow BH}^\dagger$  allows Bob (B) to decode Alice's information solely from the portion of the encoded information carried in E at  $T_0$ . Therefore, Bob obtains the state  $\rho$  before Alice prepares  $|\psi\rangle$  at  $T_1$ . The information is perfectly decoded if and only if the fidelity between  $|\psi\rangle$  and  $\rho$  is unity.

is described by an encoding unitary operator  $U_{\text{encode}} = U_{AH \rightarrow HE}$ . Here,  $U$  can also be called a *scrambler*, and the subscript labels the input subsystems (A and H) and output subsystems (H and E) of the operator. Note that the state of system H at  $T_1$  will be discussed later. The quantum information  $|\psi\rangle$  has become scrambled within the many-body entanglement of the joint system HE at  $T_2$ . Here, the output system E represents a part of the encoded information with its Hilbert space dimension also equal to  $d_A$ .

Next, the temporal direction of system E is reversed at time  $T_2$ , allowing it to travel back to  $T_0$  (a time point before  $T_1$ ) and then resume traveling forward in time.

This is achieved by utilizing a PCTC, where we introduce a chronology-violating system  $E'$ , depicted as the red curve in Fig. 1. If the initial state of  $E$  and  $E'$  at  $T_0$  is a maximally entangled state,  $E'$  can be interpreted as a mirror of  $E$  that travels backward in time [52, 53]. Furthermore, it is necessary to perform a projective (or selective) measurement on the joint system  $EE'$  at  $T_2$ , and the measurement outcome must remain consistent with itself (the same state) at  $T_0$  to obey the Novikov self-consistency principle [57]. Throughout this work, and without loss of generality, we consider the state of  $E$  and  $E'$  at  $T_0$  to be prepared as an EPR pair [77], namely

$$|\text{EPR}\rangle_{EE'} = \frac{1}{\sqrt{d_A}} \sum_{i=0}^{d_A-1} |i\rangle_E \otimes |i\rangle_{E'}. \quad (1)$$

Therefore, an EPR projective measurement must be performed at  $T_2$ , ensuring that the state of system  $E$  effectively travels backward to  $T_0$ . We denote the success probability of time travel through the PCTC (preparing and measuring  $|\text{EPR}\rangle_{EE'}$  at  $T_0$  and  $T_2$ , respectively) as  $\mathcal{P}(\psi)$  for different state  $|\psi\rangle$ .

At time  $T_0$ , a decoding operation  $U_{\text{decode}} = U_{\text{HE} \rightarrow \text{BH}}^\dagger$  is applied to the joint system  $\text{HE}$ , and then Bob ( $B$ ) subsequently receives a state  $\rho$  (generally represented as a density matrix) before  $T_1$ . To demonstrate that the final decoding process requires only  $U_{\text{HE} \rightarrow \text{BH}}^\dagger$  and the partially encoded information stored in  $E$ , we assume that the initial state of system  $H$  at  $T_0$  is maximally mixed, which does not provide any additional information. Finally, the fidelity between the states  $|\psi\rangle$  and  $\rho$  quantifies the entire decoding protocol, namely

$$\mathcal{F}(\psi) = \langle \psi | \rho | \psi \rangle. \quad (2)$$

The original information prepared by Alice is perfectly decoded if and only if the fidelity equals unity. Furthermore, the product of the success probability  $\mathcal{P}(\psi)$  and the fidelity  $\mathcal{F}(\psi)$  is lower-bounded by  $d_A^{-2}$ , namely

$$\mathcal{P}(\psi)\mathcal{F}(\psi) \geq \frac{1}{d_A^2} \quad \forall \psi \quad (3)$$

(see Appendix B for the derivation). This indicates that the original information is accurately decoded (with  $\mathcal{F} \approx 1$ ) when the success probability is sufficiently low (with  $\mathcal{P} \approx d_A^{-2}$ ) in the ideal case.

Here, we prove that our decoding protocol is mathematically equivalent, in some respects, to the one proposed by Yoshida and Kitaev [43]. In our protocol, the initial state of the many-body system  $H$  at  $T_0$  is a maximally mixed state. However, in their protocol, this initial state is derived from an entangled EPR pair between system  $H$  and an auxiliary system  $H'$ , i.e.,  $|\text{EPR}\rangle_{\text{HH}'}$ . By incorporating this constraint into our protocol, the state of the joint system  $\text{BHE}'H'$  at  $T_1$  can be described as  $|T_1\rangle_{\text{BHE}'H'} = U_{\text{HE} \rightarrow \text{BH}}^\dagger |\text{EPR}\rangle_{\text{EE}'} \otimes |\text{EPR}\rangle_{\text{HH}'}$ . The total unnormalized state after  $T_2$  can be further obtained by

applying the encoding scrambler  $U_{\text{AH} \rightarrow \text{HE}}$ , and the EPR projective measurement on system  $E$  and  $E'$ , namely

$$|T_2\rangle_{\text{BHH}'} = \langle \text{EPR} |_{\text{EE}'} U_{\text{AH} \rightarrow \text{HE}} |\psi\rangle_A \otimes |T_1\rangle_{\text{BHE}'H'}. \quad (4)$$

By introducing another auxiliary system  $B'$ , which has the same dimension as system  $B$ , the state  $|T_1\rangle_{\text{BHE}'H'}$  satisfies the following identity:

$$\begin{aligned} |T_1\rangle_{\text{BHE}'H'} &= U_{\text{HE} \rightarrow \text{BH}}^\dagger \otimes \mathbb{1}_{E'H'} |\text{EPR}\rangle_{\text{EE}'} \otimes |\text{EPR}\rangle_{\text{HH}'} \\ &= \mathbb{1}_{\text{BH}} \otimes U_{H'B' \rightarrow E'H'}^* |\text{EPR}\rangle_{\text{HH}'} \otimes |\text{EPR}\rangle_{B'B}, \end{aligned} \quad (5)$$

where  $\mathbb{1}$  is the identity operator. Therefore, by substituting Eq. (5) into Eq. (4), one obtains

$$\begin{aligned} |T_2\rangle_{\text{BHH}'} &= \langle \text{EPR} |_{\text{EE}'} U_{\text{AH} \rightarrow \text{HE}} U_{H'B' \rightarrow E'H'}^* \\ &\quad |\psi\rangle_A \otimes |\text{EPR}\rangle_{\text{HH}'} \otimes |\text{EPR}\rangle_{B'B}, \end{aligned} \quad (6)$$

which is exactly the same final unnormalized state in Yoshida and Kitaev's decoding protocol [43]. The proof under the diagrammatic notation is given in Appendix A.

Nevertheless, we emphasize that, in our protocol, the input state to the encoding scrambler  $U$  for system  $H$  must be the output from the decoding operation  $U^\dagger$ . This indicates that the decoding process must occur before the encoding process, unlike in Yoshida and Kitaev's protocol. Furthermore, their protocol requires generating multiple EPR pairs depending on the size of both systems  $H$  and  $E$ , whereas our protocol uses fewer entanglement resources. This is because we only require the preparation of a maximally mixed state for system  $H$ , and a single EPR pair between systems  $E$  and  $E'$ .

### III. QUANTUM INFORMATION SCRAMBLING AND OUT-OF-TIME-ORDER CORRELATOR

Quantum information scrambling is typically characterized by the decay of the OTOC [1, 2], defined as

$$\mathcal{O}(W, V) \equiv \langle W^\dagger(t) V^\dagger W(t) V \rangle, \quad (7)$$

where  $W$  and  $V$  are initially commuting unitary and Hermitian operators acting on separate subsystems, and the operator  $W(t) = U^\dagger W U$  is the time-evolved version of  $W$  in the Heisenberg picture according to the scrambling unitary operator  $U$ . When  $t = 0$ , the value of the OTOC  $\mathcal{O}(W, V) = 1 \forall W$  and  $V$  because  $W(0)$  commutes with  $V$ . As scrambling progresses,  $W(t)$  ceases to commute with  $V$  as it becomes increasingly nonlocal, thereby leading to the rapid decay of the OTOC.

The average value of the OTOC in Eq. (7) can be directly calculated by the success probability of time travel  $\mathcal{P}(\psi)$  in our decoding protocol:

$$\mathcal{O}_{\text{avg}} = \iint dW dV \mathcal{O}(W, V) = \int d\psi \mathcal{P}(\psi) \quad (8)$$

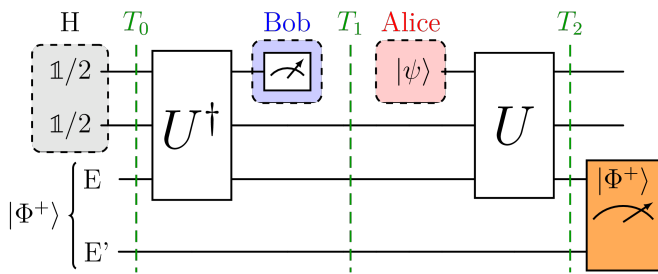


FIG. 2. Experimental demonstration of the decoding protocol using a four-qubit quantum circuit. Time progresses from  $T_0$  to  $T_2$  in the laboratory's rest frame. Initially, the system H is prepared as a two-qubit maximally mixed state, while the systems E and E' are initialized as  $|\Phi^+\rangle = (|00\rangle + |11\rangle)/\sqrt{2}$ , which is one of the Bell states. The three-qubit decoding operation  $U^\dagger$  is applied to decode the information stored solely in system E, and Bob performs quantum state tomography on qubit B before  $T_1$ . After  $T_1$ , Alice prepares the information  $|\psi\rangle$  and encodes it using the scrambler  $U$ . To complete the decoding protocol, a Bell state measurement (BSM) is performed after  $T_2$ , and Bob needs to postselect his results corresponding to the state  $|\Phi^+\rangle$ .

(see Appendix C for the derivation). Here, the double integral represents the Haar average over all unitary operators  $W$  and  $V$  on the corresponding subsystems, and the single integral averages over all initial states  $|\psi\rangle$  in our protocol. The average success probability of time travel through the PCTC decreases as the average value of the OTOC decays.

Furthermore, one can observe that the average value of the OTOC decays to  $d_A^{-2}$  for the aforementioned perfect decoding case [ $\mathcal{F}(\psi) = 1$  and  $\mathcal{P}(\psi) = d_A^{-2} \forall \psi$ ]. This indicates that *the unitary evolution  $U$  must generate sufficiently strong scrambling dynamics (which makes  $\mathcal{O}_{avg}$  decay to  $d_A^{-2}$ ) so that the information  $|\psi\rangle$  can be fully encoded through the many-body entanglement in the joint system HE at  $T_2$ , and then perfectly decoded in the past.*

#### IV. EXPERIMENTAL DEMONSTRATION

As we mentioned above, although the existence of CTCs is still vague, one can probabilistically simulate it based on postselected quantum teleportation. Here, we demonstrate our decoding protocol using a four-qubit quantum circuit, shown in Fig. 2. The circuit is implemented using Quantinuum [74] and IBMQ [75, 76] processors.

In the following, we explain the circuit in detail in the laboratory's rest frame (from  $T_0$  to  $T_2$ ). At time  $T_0$ , system H is initialized as a two-qubit maximally mixed state [ $(\mathbb{1}/2) \otimes (\mathbb{1}/2)$ ], a uniform mixture of states in the computational basis. Thus, we uniformly prepare each of the two qubits in the state  $|0\rangle$  or  $|1\rangle$ . Systems E and E' are initialized as a two-qubit EPR pair, as shown in

Eq. (1) with  $d_A = 2$ :

$$|\Phi^+\rangle_{EE'} = \frac{1}{\sqrt{2}} (|0\rangle_E \otimes |0\rangle_{E'} + |1\rangle_E \otimes |1\rangle_{E'}), \quad (9)$$

which is a Bell state [77].

After applying the decoding operation  $U^\dagger$  to the joint system HE, we perform quantum state tomography (i.e., single-qubit Pauli measurements [77]) on qubit B before  $T_1$ . To ensure the information is from the future, we reset qubit B and then prepare a pure quantum state  $|\psi\rangle$  on the same qubit (which we rename qubit A after  $T_1$ ). We emphasize that the state  $|\psi\rangle$  is prepared freely, with no knowledge of the previous measurement results. We then apply the encoding scrambler  $U$  to encode the information within the joint system HE at  $T_2$ . To complete the decoding protocol, a Bell state measurement is performed on the joint system EE' after  $T_2$ , and we postselect the outcome corresponding to  $|\Phi^+\rangle_{EE'}$  as in Eq. (9). Finally, we reconstruct the density matrix  $\rho$  from the postselected measurement results and calculate the fidelity  $\mathcal{F}(\psi)$ , given in Eq. (2), between the states  $\rho$  and  $|\psi\rangle$ , confirming that the quantum information encoded in the future has been successfully decoded from the past.

To characterize the nature of the scrambling dynamics, we repeat this protocol by encoding the six different initial states and two different scramblers:  $|\psi\rangle \in \{|x_-\rangle, |x_+\rangle, |y_-\rangle, |y_+\rangle, |z_-\rangle, |z_+\rangle\}$ , where  $|x_\pm\rangle \equiv \frac{1}{\sqrt{2}}(|0\rangle \pm |1\rangle)$ ,  $|y_\pm\rangle \equiv \frac{1}{\sqrt{2}}(|0\rangle \pm i|1\rangle)$ ,  $|z_-\rangle \equiv |1\rangle$ , and  $|z_+\rangle \equiv |0\rangle$ . For the scrambling unitary operator  $U$ , we consider the three-qubit Clifford scramblers proposed in Ref. [44]. The first Clifford scrambler, denoted as  $U_q$ , is capable of fully delocalizing arbitrary quantum information. The explicit matrix form of this unitary operator is given by:

$$U_q = \frac{1}{2\sqrt{2}} \begin{pmatrix} 1 & 1 & 1 & -1 & 1 & -1 & -1 & -1 \\ 1 & -1 & 1 & 1 & 1 & 1 & -1 & 1 \\ 1 & 1 & -1 & 1 & 1 & -1 & 1 & 1 \\ -1 & 1 & 1 & 1 & -1 & -1 & -1 & 1 \\ 1 & 1 & 1 & -1 & -1 & 1 & 1 & 1 \\ -1 & 1 & -1 & -1 & 1 & 1 & -1 & 1 \\ -1 & -1 & 1 & -1 & 1 & -1 & 1 & 1 \\ -1 & 1 & 1 & 1 & 1 & 1 & 1 & -1 \end{pmatrix}. \quad (10)$$

The success probability for an arbitrary state  $|\psi\rangle$  under the scrambler  $U_q$  is  $\mathcal{P}(\psi) = 0.25$ . According to Eq. (3), this leads to an estimated fidelity of unity for any state  $|\psi\rangle$ , indicating perfect decoding.

To show the strength of  $U_q$ , we compare it with another Clifford scrambler, denoted as  $U_c$ , which only scrambles classical information:

$$U_c = \text{diag}(1, 1, 1, -1, 1, -1, -1, -1). \quad (11)$$

In this case, the average success probability of the PCTC  $\mathcal{P}_{avg} = 0.5$ , resulting in a lower bound on the fidelity of 0.5. Only states  $|\psi\rangle$  prepared in  $|0\rangle$  or  $|1\rangle$  can be perfectly decoded, while the fidelity of all other states is 0.5. The

TABLE I. Experimental results of the decoding fidelity ( $\mathcal{F}$ ) and the success probability of time travel ( $\mathcal{P}$ ) for different initial states  $|\psi\rangle$  under Clifford scramblers ( $U_q$  and  $U_c$ ). As shown in Eq. (8), the average value of the out-of-time-order correlator ( $\mathcal{O}_{\text{avg}}$ ) equals the average value of  $\mathcal{P}(\psi)$ .

$ \psi\rangle$	$U_q$ (Quantinuum)		$U_q$ (IBMQ)		$U_c$ (IBMQ)	
	$\mathcal{F}(\psi)$	$\mathcal{P}(\psi)$	$\mathcal{F}(\psi)$	$\mathcal{P}(\psi)$	$\mathcal{F}(\psi)$	$\mathcal{P}(\psi)$
$ x_-\rangle$	0.976	0.258	0.8320	0.2519	0.5021	0.4430
$ x_+\rangle$	0.986	0.249	0.8219	0.2619	0.5014	0.4440
$ y_-\rangle$	0.990	0.243	0.8681	0.2592	0.4949	0.4454
$ y_+\rangle$	0.988	0.256	0.8506	0.2578	0.5082	0.4406
$ z_-\rangle$	0.983	0.253	0.8479	0.2566	0.9092	0.4405
$ z_+\rangle$	0.987	0.252	0.8512	0.2564	0.9130	0.4461
Average	0.985	0.252	0.8453	0.2573	0.6381	0.4433

circuit decompositions for both Clifford scramblers ( $U_q$  and  $U_c$ ) are given in Appendix D.

We performed the experiments using the *H1-1* processor from Quantinuum [74] and the *ibm\_torino* processor from IBMQ [75, 76]. The topology and calibration data are also presented in Appendix D. The experimental results, as shown in Table I, are obtained through 4,000 and 40,000 shots for each measurement procedure in the state tomography using the *H1-1* and *ibm\_torino*, respectively. For both processors, when  $U_q$  is employed as the scrambler in the protocol, we observe that the success probability of time travel  $\mathcal{P}(\psi)$  approximately approaches  $d_A^{-2} = 0.25$  for all initial states  $|\psi\rangle$ , which also means that  $\mathcal{O}_{\text{avg}} \approx 0.25$  due to Eq. (8). Due to the strong QIS  $U_q$ , the decoding protocol succeeds with an average fidelity of 0.985 (0.8453) using *H1-1* (*ibm\_torino*). Additionally, it can be observed that the average fidelity achieved on the *H1-1* processor is higher than that on *ibm\_torino*. This is attributed to the *H1-1* processor's longer qubit relaxation and decoherence times, as well as lower readout and gate error rates (see Appendix D for the calibration data of both processors).

In contrast, applying the same protocol with the scrambler  $U_c$  using *ibm\_torino* results in a low decoding fidelity. Although the fidelity for states  $|z_{\pm}\rangle$  remains relatively high (around 0.91), the fidelity drops significantly to around 0.5 for other states ( $|x_{\pm}\rangle$  and  $|y_{\pm}\rangle$ ). This indicates that  $U_c$  only has the capability to scramble classical information ( $|z_{\pm}\rangle$ ) instead of general quantum information. The large value of  $\mathcal{O}_{\text{avg}} = \mathcal{P}_{\text{avg}} = 0.4433$  further supports this conclusion.

## V. CONCLUSIONS

We have proposed a protocol and experimentally demonstrated it on both Quantinuum and IBM Quantum processors, leveraging QIS and PCTCs to transmit and decode encrypted quantum information from the future into the past. Although QIS delocalizes the original

quantum information through many-body entanglement, we can still retrieve it by sending part of the scrambled information into the past. Time travel can be simulated through PCTCs, and its average success probability is directly related to the average value of OTOC in QIS. Notably, we observe that the perfect decoding fidelity of our protocol requires strong QIS, which corresponds to a sufficiently low average value of the OTOC.

To substantiate our theoretical framework, we conducted a proof-of-principle experiment, highlighting the essential roles that QIS and PCTCs play in the success of decoding an encrypted message from the future. Importantly, our protocol preserves the causality of information [78]. Sending a secret to the past via PCTCs is like ouroboros, a serpent devouring its own tail. Any attempt to alter the past is a futile endeavor because whatever happened, happened.

Our work paves the way for several intriguing future research directions. First, integrating our protocol with existing quantum key distribution protocols could yield new cryptographic applications that leverage the time-travel aspects for enhanced secure communication. Second, our protocol allows the estimation of the average value of the OTOC for arbitrary QIS using only one additional entangled EPR pair. While our demonstration utilizes a three-qubit scrambler, exploring more complex scrambling dynamics could enhance the understanding of the relationship between the decoding fidelity and different types of QIS, potentially optimizing the protocol further. Finally, our protocol establishes a connection between QIS and PCTCs, exploring insights related to black holes, wormholes, and time travel.

## ACKNOWLEDGMENTS

The authors acknowledge fruitful discussions with Chia-Yi Ju and Gelo Noel Tabia. The authors also acknowledge the NTU-IBM Q Hub, IBM Quantum, and Cloud Computing Center for Quantum Science & Technology at NCKU for providing us a platform to implement the experiments. YTH acknowledges the support of the National Science and Technology Council, Taiwan (NSTC Grants No. 113-2917-I-006-024). A.M. was supported by the Polish National Science Centre (NCN) under the Maestro Grant No. DEC-2019/34/A/ST2/00081. GYC acknowledges the support of the National Science and Technology Council, Taiwan (NSTC Grants No. 113-2112-M-005-008). F.N. is supported in part by: Nippon Telegraph and Telephone Corporation (NTT) Research, the Japan Science and Technology Agency (JST) [via the CREST Quantum Frontiers program Grant No. JP-MJCR24I2, the Quantum Leap Flagship Program (Q-LEAP), and the Moonshot R&D Grant Number JP-MJMS2061], and the Office of Naval Research (ONR) Global (via Grant No. N62909-23-1-2074). YNC acknowledges the support of the National Center for Theoretical Sciences and the National Science and Technology

Council, Taiwan (NSTC Grants No. 113-2123-M-006-001).

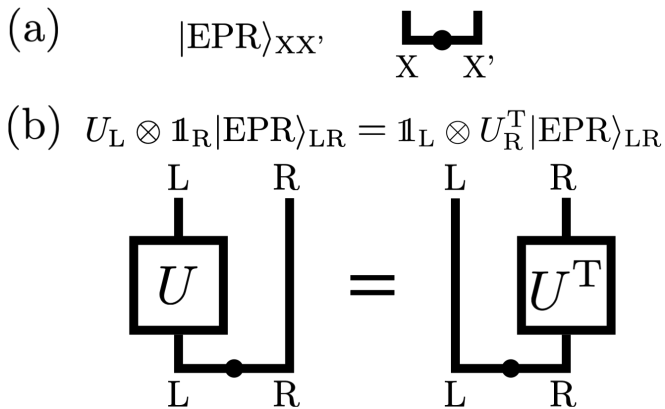


FIG. 3. Diagrammatic notations: (a) An EPR state. (b) A local unitary operator  $U$  acting on the left (L) of the EPR state is equivalent to its transpose (T) acting on the right (R) of the EPR state.

### Appendix A: Diagrammatic proof of the equivalence between two decoding protocols

In this Appendix, we provide a proof using diagrammatic notation to demonstrate the equivalence between our decoding protocol, presented in the main text, and the protocol proposed by Yoshida and Kitaev [43]. We begin by introducing the diagrammatic notation of a general EPR state shared between a system X and an auxiliary system X' with dimension  $d$ :

$$|\text{EPR}\rangle_{\text{XX}'} = \frac{1}{\sqrt{d}} \sum_{j=0}^{d-1} |j\rangle_{\text{X}} \otimes |j\rangle_{\text{X}'}, \quad (\text{A1})$$

as shown in Fig. 3(a). The open ends of the wires, pointing upward, represent a vector (ket state), and the black dot in the middle of the wire indicates that the EPR pair is normalized (scaled by  $1/\sqrt{d}$ ). A key element of this proof is the following identity, which holds when an arbitrary local unitary  $U$  is applied to an EPR pair:

$$U_{\text{L}} \otimes \mathbb{1}_{\text{R}} |\text{EPR}\rangle_{\text{LR}} = \mathbb{1}_{\text{L}} \otimes U_{\text{R}}^{\text{T}} |\text{EPR}\rangle_{\text{LR}}, \quad (\text{A2})$$

as shown in Fig. 3(b). Here, the superscript T represents the transpose of an operator, and  $\mathbb{1}$  is the identity operator.

The diagrammatic notation of our decoding protocol is shown in Fig. 4(a). As mentioned in the main text, the system H is generally a many-body system. Additionally, the initial state of H in our protocol is a maximally mixed state which does not provide any additional information for the final decoding process, i.e.,  $U_{\text{HE} \rightarrow \text{BH}}^{\dagger}$  decodes the information solely carried in system E at  $T_0$ . However, in Yoshida and Kitaev's protocol [43], the initial state originates from an EPR pair between the system H and an

auxiliary system H', i.e.,  $|\text{EPR}\rangle_{\text{HH}'}$ . Incorporating this constraint into our protocol, as presented in the main text, the final unnormalized state  $|f(\psi)\rangle$  in our protocol, corresponding to the input quantum information  $|\psi\rangle$  from Alice, can be expressed as

$$\begin{aligned} |f(\psi)\rangle_{\text{BHH}'} &= \langle \text{EPR} |_{\text{AB}'} U_{\text{AH}} U_{\text{BH}}^{\dagger} |\psi\rangle_{\text{A}} \otimes |\text{EPR}\rangle_{\text{BB}'} \otimes |\text{EPR}\rangle_{\text{HH}'}. \end{aligned} \quad (\text{A3})$$

Here, without loss of generality, we relabel the input system E (at time  $T_0$ ), output system E (at time  $T_2$ ), and the chronology-violating system E' from the main text as B, A, and B', respectively. This relabeling is justified because, from the perspective of PCTCs, all these systems represent the same system that carries the information at different time points, or travels in different directions in time.

Additionally, for simplicity, we rearrange both the input and output Hilbert spaces into the same order as AHBB'H' in the diagrammatic notation, as shown in Fig. 4(b). Note that although the diagrammatic notation of  $|\text{EPR}\rangle_{\text{HH}'}$  in Fig. 4(b) appears as a single wire, it actually represents multiple EPR pairs shared between the corresponding subsystems of H and H'.

Using the equality given in Eq. (A2), we can also replace the decoding unitary operation  $U_{\text{BH}}^{\dagger} \otimes \mathbb{1}_{\text{B}'\text{H}'}$  with  $\mathbb{1}_{\text{BH}} \otimes U_{\text{B}'\text{H}'}^*$  in Eq. (A3), namely

$$\begin{aligned} |f(\psi)\rangle_{\text{BHH}'} &= \langle \text{EPR} |_{\text{AB}'} U_{\text{AH}} U_{\text{B}'\text{H}'}^* |\psi\rangle_{\text{A}} \otimes |\text{EPR}\rangle_{\text{BB}'} \otimes |\text{EPR}\rangle_{\text{HH}'}, \end{aligned} \quad (\text{A4})$$

for which the corresponding diagrammatic notation is given in Fig. 4(c). After rearranging the input Hilbert space order to AHH'B'B and the output Hilbert space order to HAB'H'B in the diagrammatic notation [as shown in Fig. 4(d)], the unnormalized state  $|f\rangle$  is identical to the one presented in Yoshida and Kitaev's decoding protocol [43]. Consequently, the normalized decoded state can be expressed as

$$\rho_{\text{B}} = \frac{\text{Tr}_{\text{HH}'} [|f(\psi)\rangle \langle f(\psi)|_{\text{BHH}'}]}{\mathcal{P}(\psi)}, \quad (\text{A5})$$

where  $\mathcal{P}(\psi)$  denotes the success probability of a PCTC:

$$\mathcal{P}(\psi) = \langle f(\psi) | f(\psi) \rangle. \quad (\text{A6})$$

Finally, one can quantify the entire decoding protocol via the fidelity between the states  $|\psi\rangle$  and  $\rho_{\text{B}}$ , namely

$$\mathcal{F}(\psi) = \langle \psi | \rho_{\text{B}} | \psi \rangle. \quad (\text{A7})$$

### Appendix B: A lower bound for the product of the PCTC success probability and decoding fidelity

In this Appendix, we demonstrate that the product of the PCTC success probability [ $\mathcal{P}$  in Eq. (A6)] and the

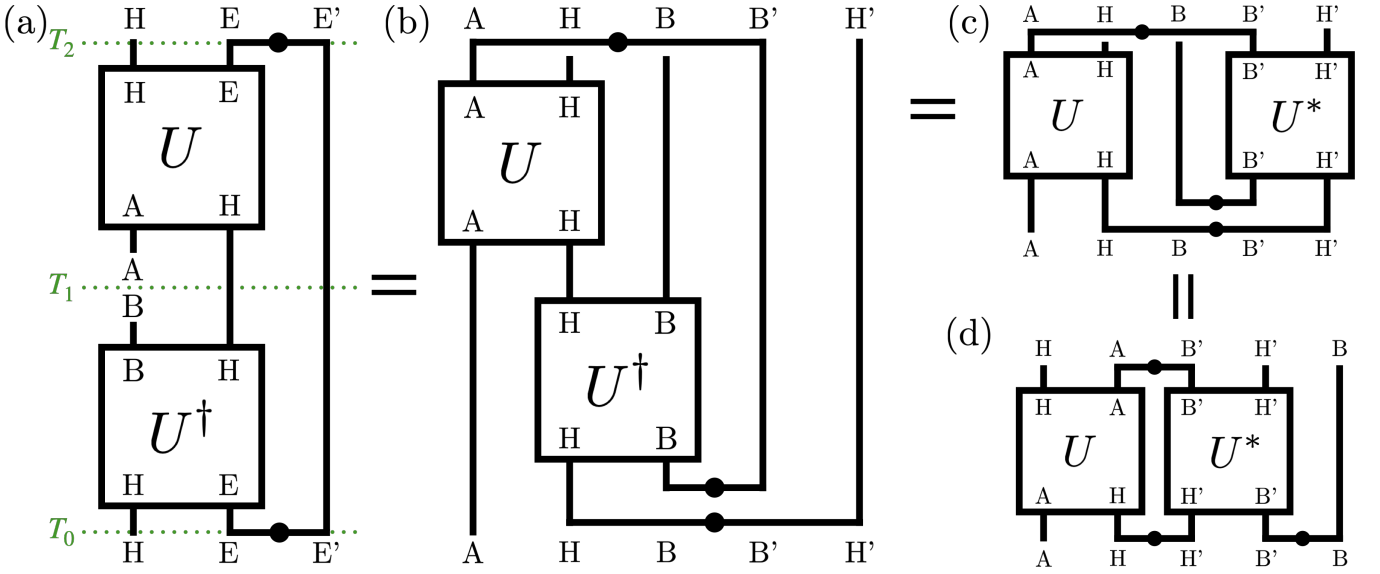


FIG. 4. Proof of the equivalence of protocols using diagrammatic notation. (a) The diagram of the decoding protocol, where time progresses from  $T_0$  to  $T_2$  in the laboratory's rest frame. (b) We introduce the purification  $|\text{EPR}\rangle_{\text{HH}'}$  for the initial state of the many-body system  $H$ , which is a maximally mixed state, with its reference system  $H'$ . For simplicity, we relabel the input system  $E$  (at time  $T_0$ ), output system  $E$  (at time  $T_2$ ), and system  $E'$  as  $B, A,$  and  $B'$ , respectively. The equivalence between the diagrams in (b) and (c) follows from the properties of the EPR state, as described in Eq. (A2). (d) Diagram obtained by rearranging the input and output Hilbert space order from the diagram in (c).

decoding fidelity  $[\mathcal{F}$  in Eq. (A7)] in our decoding protocol is lower-bounded by  $d_A^{-2}$  for an arbitrary encoded state  $|\psi\rangle$ . Here,  $d_A$  denotes the Hilbert space dimension of

the original input quantum information  $|\psi\rangle$  from Alice. We begin by substituting Eq. (A5) into Eq. (A7) and multiplying by  $\mathcal{P}(\psi)$ , namely

$$\begin{aligned}
\mathcal{P}(\psi)\mathcal{F}(\psi) &= \langle\psi|_B \left( \text{Tr}_{\text{HH}'} [ |f(\psi)\rangle \langle f(\psi)|_{\text{BHH}'} ] \right) |\psi\rangle_B \\
&\geq \langle\psi|_B \left( \text{Tr}_{\text{HH}'} [ |\text{EPR}\rangle \langle \text{EPR}|_{\text{HH}'} \cdot |f(\psi)\rangle \langle f(\psi)|_{\text{BHH}'} ] \right) |\psi\rangle_B \\
&= \langle\psi|_B \otimes \langle \text{EPR}|_{\text{HH}'} \left( |f(\psi)\rangle \langle f(\psi)|_{\text{BHH}'} \right) |\psi\rangle_B \otimes |\text{EPR}\rangle_{\text{HH}'} \\
&= \left| \langle\psi|_B \otimes \langle \text{EPR}|_{\text{HH}'} \cdot |f(\psi)\rangle_{\text{BHH}'} \right|^2.
\end{aligned} \tag{B1}$$

The above inequality holds because we also perform an EPR projective measurement on the joint system  $\text{HH}'$

before tracing them out. Next, by substituting Eq. (A4) into Eq. (B1), one obtains

$$\mathcal{P}(\psi)\mathcal{F}(\psi) \geq \left| \langle\psi|_B \otimes \langle \text{EPR}|_{\text{AB}'} \otimes \langle \text{EPR}|_{\text{HH}'} U_{\text{AH}} U_{\text{B}'\text{H}'}^* |\psi\rangle_A \otimes |\text{EPR}\rangle_{\text{BB}'} \otimes |\text{EPR}\rangle_{\text{HH}'} \right|^2. \tag{B2}$$

Note that  $U_{\text{AH}}$  and  $U_{\text{B}'\text{H}'}^*$  commute, and we can apply the equality given in Eq. (A2) once more to replace  $U_{\text{B}'\text{H}'}^*$

with  $U_{\text{AH}}^\dagger$  since

$$\begin{aligned}
&\langle \text{EPR}|_{\text{AB}'} \otimes \langle \text{EPR}|_{\text{HH}'} \mathbb{1}_{\text{AH}} \otimes U_{\text{B}'\text{H}'}^* \\
&= \langle \text{EPR}|_{\text{AB}'} \otimes \langle \text{EPR}|_{\text{HH}'} U_{\text{AH}}^\dagger \otimes \mathbb{1}_{\text{B}'\text{H}'}.
\end{aligned} \tag{B3}$$

Thus, with  $U_{\text{AH}}^\dagger U_{\text{AH}} = \mathbb{1}_{\text{AH}}$ , Eq. (B2) results in

$$\begin{aligned}
\mathcal{P}(\psi)\mathcal{F}(\psi) &\geq \left| \langle \psi |_{\text{B}} \otimes \langle \text{EPR} |_{\text{AB}'} \cdot | \psi \rangle_{\text{A}} \otimes | \text{EPR} \rangle_{\text{BB}'} \right|^2 \\
&= \left| \frac{1}{\sqrt{d_{\text{A}}}} \frac{1}{\sqrt{d_{\text{A}}}} \sum_{i=0}^{d_{\text{A}}-1} \sum_{j=0}^{d_{\text{A}}-1} \langle i | \psi \rangle_{\text{A}} \cdot \langle \psi | j \rangle_{\text{B}} \cdot \langle i | j \rangle_{\text{B}'} \right|^2 \\
&= \left| \frac{1}{d_{\text{A}}} \sum_{i=0}^{d_{\text{A}}-1} \langle i | \psi \rangle \langle \psi | i \rangle \right|^2 \\
&= \frac{1}{d_{\text{A}}^2} \quad \forall \quad \psi. \tag{B4}
\end{aligned}$$

We have completed the proof that a lower bound of  $\mathcal{P}(\psi)\mathcal{F}(\psi)$  for an arbitrary initial state  $|\psi\rangle$  is  $d_{\text{A}}^{-2}$ .  $\blacksquare$

Note that a similar proof for the above protocol can also be found in Ref. [43].

### Appendix C: Directly observing QIS from the average success probability of the PCTC

The phenomenon of quantum information scrambling is typically characterized by the decay of the out-of-time-order correlator (OTOC) [1, 2]. Here, we show that the average success probability of the PCTC in our protocol equals to the average value of the OTOC ( $\mathcal{O}_{\text{avg}}$ ). We begin by substituting Eq. (A4) into Eq. (A6) and averaging over all possible input states  $\psi$ , namely

$$\begin{aligned}
\int d\psi \mathcal{P}(\psi) &= \int d\psi \langle f(\psi) | f(\psi) \rangle \\
&= \int d\psi \langle \psi |_{\text{A}} \otimes \langle \text{EPR} |_{\text{BB}'} \otimes \langle \text{EPR} |_{\text{HH}'} U_{\text{B}'\text{H}'}^{\text{T}} U_{\text{AH}}^\dagger | \text{EPR} \rangle \langle \text{EPR} |_{\text{AB}'} U_{\text{AH}} U_{\text{B}'\text{H}'}^* | \psi \rangle_{\text{A}} \otimes | \text{EPR} \rangle_{\text{BB}'} \otimes | \text{EPR} \rangle_{\text{HH}'} \rangle. \tag{C1}
\end{aligned}$$

Note that the above EPR projection operator  $|\text{EPR}\rangle\langle\text{EPR}|_{\text{AB}'}$  can be represented as a Haar average over all local unitary operators  $W$  acting on the subsystems A and B' [44, 79]:

$$|\text{EPR}\rangle\langle\text{EPR}|_{\text{AB}'} = \int dW W_{\text{A}} \otimes W_{\text{B}'}^*. \tag{C2}$$

Next, by substituting Eq. (C2) into Eq. (C1), one obtains

$$\begin{aligned}
\int d\psi \mathcal{P}(\psi) &= \iint dW d\psi \langle \psi |_{\text{A}} \otimes \langle \text{EPR} |_{\text{BB}'} \otimes \langle \text{EPR} |_{\text{HH}'} U_{\text{B}'\text{H}'}^{\text{T}} U_{\text{AH}}^\dagger W_{\text{A}} W_{\text{B}'}^* U_{\text{AH}} U_{\text{B}'\text{H}'}^* | \psi \rangle_{\text{A}} \otimes | \text{EPR} \rangle_{\text{BB}'} \otimes | \text{EPR} \rangle_{\text{HH}'} \\
&= \iint dW d\psi \langle \psi |_{\text{A}} \otimes \langle \text{EPR} |_{\text{BB}'} \otimes \langle \text{EPR} |_{\text{HH}'} (U_{\text{B}'\text{H}'}^{\text{T}} W_{\text{B}'}^* U_{\text{B}'\text{H}'}^*) (U_{\text{AH}}^\dagger W_{\text{A}} U_{\text{AH}}) | \psi \rangle_{\text{A}} \otimes | \text{EPR} \rangle_{\text{BB}'} \otimes | \text{EPR} \rangle_{\text{HH}'} \\
&= \iint dW d\psi \langle \psi |_{\text{A}} \otimes \langle \text{EPR} |_{\text{BB}'} \otimes \langle \text{EPR} |_{\text{HH}'} (U_{\text{B}'\text{H}'}^\dagger W_{\text{B}'}^\dagger U_{\text{B}'\text{H}'}^{\text{T}})^\dagger (U_{\text{AH}}^\dagger W_{\text{A}} U_{\text{AH}}) | \psi \rangle_{\text{A}} \otimes | \text{EPR} \rangle_{\text{BB}'} \otimes | \text{EPR} \rangle_{\text{HH}'} \\
&= \iint dW d\psi \langle \psi |_{\text{A}} \otimes \langle \text{EPR} |_{\text{BB}'} \otimes \langle \text{EPR} |_{\text{HH}'} (U_{\text{BH}}^\dagger W_{\text{B}}^\dagger U_{\text{BH}}) (U_{\text{AH}}^\dagger W_{\text{A}} U_{\text{AH}}) | \psi \rangle_{\text{A}} \otimes | \text{EPR} \rangle_{\text{BB}'} \otimes | \text{EPR} \rangle_{\text{HH}'} \rangle. \tag{C3}
\end{aligned}$$

Here, the last equality follows from Eq. (A2). We can define the time-evolved version of  $W$  in the Heisenberg picture according to the scrambling unitary operator  $U$ , i.e.,  $W_{\text{A}}(t) = U_{\text{AH}}^\dagger W_{\text{A}} U_{\text{AH}}$  and  $W_{\text{B}}^\dagger(t) = U_{\text{BH}}^\dagger W_{\text{B}}^\dagger U_{\text{BH}}$ . Furthermore, the input state  $|\psi\rangle_{\text{A}}$  can be generated by a

unitary operator  $V$  acting on a fixed initial state  $|\phi_0\rangle_{\text{A}}$ , i.e.,  $|\psi\rangle_{\text{A}} = V_{\text{A}} |\phi_0\rangle_{\text{A}}$  and  $V_{\text{A}} = |\psi\rangle\langle\phi_0|_{\text{A}}$ . Thus, the average over  $\psi$  can be performed by integrating over  $V$ , namely



$$\begin{aligned}
\int d\psi \mathcal{P}(\psi) &= \iint dW dV \langle \phi_0|_A \otimes \langle \text{EPR}|_{\text{BB}'} \otimes \langle \text{EPR}|_{\text{HH}'} W_B^\dagger(t) V_A^\dagger W_A(t) V_A |\phi_0\rangle_A \otimes |\text{EPR}\rangle_{\text{BB}'} \otimes |\text{EPR}\rangle_{\text{HH}'} \\
&= \iint dW dV \langle W_B^\dagger(t) V_A^\dagger W_A(t) V_A \rangle \\
&= \mathcal{O}_{\text{avg}}.
\end{aligned} \tag{C4}$$

This completes the proof that the average value of the OTOC ( $\mathcal{O}_{\text{avg}}$ ) is equal to the average success probability of the PCTC in our protocol. ■

Note that a similar proof can also be found in Refs. [44, 79].

As discussed in Appendix A, we relabel certain systems to simplify the previous proof. To better illustrate the

connection between OTOCs and PCTCs through our decoding protocol, we revert to using the same labels and notations as in the main text. Because the EPR projection operator is applied to the joint system  $EE'$  at  $T_2$  [as shown in Fig. 4(a)], the unitary operator  $W$  in Eq. (C2) should act on system E. Therefore, the OTOC  $\langle W^\dagger(t) V^\dagger W(t) V \rangle$  in Eq. (C4) can be interpreted as the overlap between the following two states:

$$W_E(t) V_A |\phi_0\rangle_A \otimes |\text{EPR}\rangle_{\text{EE}'} \otimes |\text{EPR}\rangle_{\text{HH}'} = U_{\text{HE} \rightarrow \text{BH}}^\dagger W_E U_{\text{AH} \rightarrow \text{HE}} V_A |\phi_0\rangle_A \otimes |\text{EPR}\rangle_{\text{EE}'} \otimes |\text{EPR}\rangle_{\text{HH}'}, \tag{C5}$$

$$V_A W_E(t) |\phi_0\rangle_A \otimes |\text{EPR}\rangle_{\text{EE}'} \otimes |\text{EPR}\rangle_{\text{HH}'} = V_A U_{\text{HE} \rightarrow \text{AH}}^\dagger W_E U_{\text{BH} \rightarrow \text{HE}} |\phi_0\rangle_B \otimes |\text{EPR}\rangle_{\text{EE}'} \otimes |\text{EPR}\rangle_{\text{HH}'}. \tag{C6}$$

The state in Eq. (C5) follows the standard procedure of our protocol. Starting at  $T_1$ , Alice prepares the state  $|\psi\rangle_A$  by applying the unitary operator  $V_A$  on the initial state  $|\phi_0\rangle_A$ , and then the information is encoded in the joint system HE at time  $T_2$  by the encoding scrambler  $U_{\text{AH} \rightarrow \text{HE}}$ . A unitary operator  $W_E$  is then applied to system E, which can be regarded as a perturbation from the perspective of QIS. After system E travels backward in time from  $T_2$  to  $T_0$  through the PCTC, the decoding operation  $U_{\text{HE} \rightarrow \text{BH}}^\dagger$  is applied, and Bob receives the state.

In contrast, the state in Eq. (C6) represents the inverse version of our protocol, where the direction of all timelines (as indicated by the arrows in Fig. 1) is reversed. As time proceeds backward from  $T_1$  to  $T_0$ , Bob encodes the state  $|\phi_0\rangle_B$  into the joint system HE using the scrambling operation  $(U_{\text{BH} \rightarrow \text{HE}}^\dagger)^\dagger = U_{\text{BH} \rightarrow \text{HE}}$ . After system E travels forward in time from  $T_0$  to  $T_2$  through the PCTC, the perturbation  $W_E$  is applied to system E, and the temporal direction is again reversed at  $T_2$ . As time proceeds backward from  $T_2$  to  $T_1$ , the decoding operation  $U_{\text{HE} \rightarrow \text{AH}}^\dagger$  is applied, and Alice finally applies the unitary operator  $V_A$  to her state.

Consequently, the value of the OTOC for the specific unitary operators  $W_E$  and  $V_A$  can be determined by calculating the overlap between the output states from the standard and inverse versions of our decoding protocol. Nevertheless, for the average value of the OTOC ( $\mathcal{O}_{\text{avg}}$ ), we highlight that it can be directly obtained from the average success probability of the PCTC in our decoding protocol using Eq. (C4), without the need for the Haar averaging over all possible operators  $W_E$  and  $V_A$ .

#### Appendix D: Circuit decompositions of the three-qubit Clifford scrambling unitary operators for Quantinuum and IBM Quantum processors

In this Appendix, we provide the circuit decompositions for the three-qubit Clifford scrambling unitary operators ( $U_q$  and  $U_c$ ) used in the main text. In Ref. [44], the quantum information scrambler  $U_q$  can be represented by several Hadamard gates, along with the controlled- $Z$  gates, as shown in Fig. 5(a). In contrast, the classical information scrambler  $U_c$  only requires the three controlled- $Z$  gates, as shown in Fig. 5(b).

We performed the experiment on the Quantinuum *H1-1* quantum charge-coupled processor, which features 20 trapped-ion ( $^{171}\text{Yb}^+$ ) qubits with all-to-all connectivity [74]. This allows the circuit shown in Fig. 5(a) to be executed directly on the *H1-1* processor. The calibration data for *H1-1* is presented in Table II.

TABLE II. Calibration data (obtained on Apr. 10, 2024) for the Quantinuum processor *H1-1* used in our experiments.

Relaxation time	$\gg 1$ minute
Decoherence time	$\approx 4$ seconds
Readout error	$2.5 \times 10^{-3}$
Single-qubit gate error	$2.1 \times 10^{-5}$
Two-qubit gate error	$8.8 \times 10^{-4}$

We also conduct the experiment on an IBM Quantum processor called *ibm.torino*, which contains 133 super-

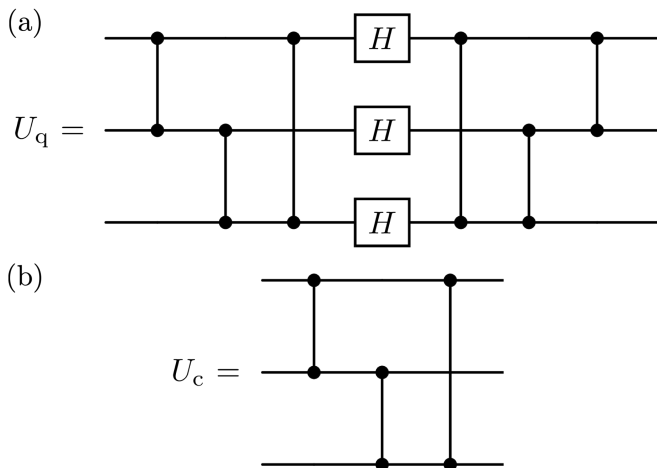


FIG. 5. Circuit representation of two Clifford scramblers. (a) The quantum information scrambling unitary operator  $U_q$  (b) The classical information scrambling unitary operator  $U_c$ .

conducting qubits [75, 76]. The topology of the qubits used in the experiment is illustrated in Fig. 6(a), and the corresponding calibration data for each used qubit is presented in Table III. However, the two-qubit gates in Fig. 5 do not match the topology shown in Fig. 6(a). Therefore, we provide circuit decompositions in Fig. 6(b) and Fig. 6(c) to align with the topology of *ibm\_torino*, and the corresponding decomposition of each Hadamard gate is shown in Fig. 6(d).

- 
- [1] S. Xu and B. Swingle, Scrambling Dynamics and Out-of-Time-Ordered Correlators in Quantum Many-Body Systems, *PRX Quantum* **5**, 010201 (2024).
- [2] B. Swingle, Unscrambling the physics of out-of-time-order correlators, *Nat. Phys.* **14**, 988 (2018).
- [3] E. Iyoda and T. Sagawa, Scrambling of quantum information in quantum many-body systems, *Phys. Rev. A* **97**, 042330 (2018).
- [4] D. Ding, P. Hayden, and M. Walter, Conditional mutual information of bipartite unitaries and scrambling, *J. High Energy Phys.* **2016**, 145 (2016).
- [5] N. Yunger Halpern, B. Swingle, and J. Dressel, Quasiprobability behind the out-of-time-ordered correlator, *Phys. Rev. A* **97**, 042105 (2018).
- [6] S. Pappalardi, A. Russomanno, B. Žunković, F. Iemini, A. Silva, and R. Fazio, Scrambling and entanglement spreading in long-range spin chains, *Phys. Rev. B* **98**, 134303 (2018).
- [7] A. Touil and S. Deffner, Quantum scrambling and the growth of mutual information, *Quantum Sci. Technol.* **5**, 035005 (2020).
- [8] J.-D. Lin, W.-Y. Lin, H.-Y. Ku, N. Lambert, Y.-N. Chen, and F. Nori, Quantum steering as a witness of quantum scrambling, *Phys. Rev. A* **104**, 022614 (2021).
- [9] K. K. Sharma and V. P. Gerdt, Quantum information scrambling and entanglement in bipartite quantum states, *Quantum Inf. Process.* **20**, 195 (2021).
- [10] J. Harris, B. Yan, and N. A. Sinitsyn, Benchmarking Information Scrambling, *Phys. Rev. Lett.* **129**, 050602 (2022).
- [11] Q. Zhu *et al.*, Observation of Thermalization and Information Scrambling in a Superconducting Quantum Processor, *Phys. Rev. Lett.* **128**, 160502 (2022).
- [12] G. L. Monaco, L. Innocenti, D. Cilluffo, D. A. Chisholm, S. Lorenzo, and G. M. Palma, An operational definition of quantum information scrambling, [arXiv:2312.11619](https://arxiv.org/abs/2312.11619) (2023).
- [13] R. J. Garcia, K. Bu, and A. Jaffe, Resource theory of quantum scrambling, *Proc. Natl. Acad. Sci.* **120**, e2217031120 (2023).
- [14] P. Hosur, X.-L. Qi, D. A. Roberts, and B. Yoshida, Chaos in quantum channels, *J. High Energy Phys.* **2016**, 4 (2016).
- [15] A. Seshadri, V. Madhok, and A. Lakshminarayan, Tripartite mutual information, entanglement, and scrambling in permutation symmetric systems with an application to quantum chaos, *Phys. Rev. E* **98**, 052205 (2018).
- [16] N. Dowling, P. Kos, and K. Modi, Scrambling Is Necessary but Not Sufficient for Chaos, *Phys. Rev. Lett.* **131**, 180403 (2023).
- [17] J. Maldacena and D. Stanford, Remarks on the Sachdev-Ye-Kitaev model, *Phys. Rev. D* **94**, 106002 (2016).
- [18] A. Nahum, J. Ruhman, S. Vijay, and J. Haah, Quantum entanglement growth under random unitary dynamics, *Phys. Rev. X* **7**, 031016 (2017).
- [19] C. W. von Keyserlingk, T. Rakovszky, F. Pollmann, and S. L. Sondhi, Operator hydrodynamics, OTOCs, and entanglement growth in systems without conservation laws, *Phys. Rev. X* **8**, 021013 (2018).
- [20] J. Cotler, N. Hunter-Jones, J. Liu, and B. Yoshida, Chaos, complexity, and random matrices, *J. High Energy Phys.* **2017**, 48 (2017).
- [21] R. Fan, P. Zhang, H. Shen, and H. Zhai, Out-of-time-order correlation for many-body localization, *Sci. Bull.* **62**, 707 (2017).
- [22] Y. Gu, X.-L. Qi, and D. Stanford, Local criticality, diffusion and chaos in generalized Sachdev-Ye-Kitaev models, *J. High Energy Phys.* **2017**, 125 (2017).
- [23] V. Khemani, A. Vishwanath, and D. A. Huse, Operator spreading and the emergence of dissipative hydrodynamics under unitary evolution with conservation laws, *Phys. Rev. X* **8**, 031057 (2018).
- [24] M. Zonnios, J. Levinsen, M. M. Parish, F. A. Pollock, and K. Modi, Signatures of Quantum Chaos in an Out-of-Time-Order Tensor, *Phys. Rev. Lett.* **128**, 150601 (2022).
- [25] P. Hayden and J. Preskill, Black holes as mirrors: Quantum information in random subsystems, *J. High Energy Phys.* **2007**, 120 (2007).

TABLE III. Calibration data (obtained on Sep. 26, 2024) for the IBM Quantum processor *ibm\_torino* used in our experiments. The qubit index refer to those in Fig. 6(a). Here,  $R_Z$  is a single-qubit rotation gate around the  $Z$ -axis, and  $\sqrt{X}$  is the square root of Pauli- $X$  gate. The average two-qubit (controlled- $Z$ ) gate error is estimated to be  $1.62 \times 10^{-3}$ .

System label (at time $T_0$ )	Qubit index	Relaxation time ( $\mu\text{s}$ )	Decoherence time ( $\mu\text{s}$ )	Frequency (GHz)	Anharmonicity (GHz)	Errors		
						Readout	$R_Z$	$\sqrt{X}$
H	87	293.88	256.22	0	0	$6.30 \times 10^{-3}$	0	$1.44 \times 10^{-4}$
	88	280.95	403.23	0	0	$2.54 \times 10^{-2}$	0	$1.49 \times 10^{-4}$
E	94	274.41	272.24	0	0	$1.07 \times 10^{-2}$	0	$1.52 \times 10^{-4}$
E'	107	88.68	105.80	0	0	$2.86 \times 10^{-2}$	0	$5.16 \times 10^{-4}$

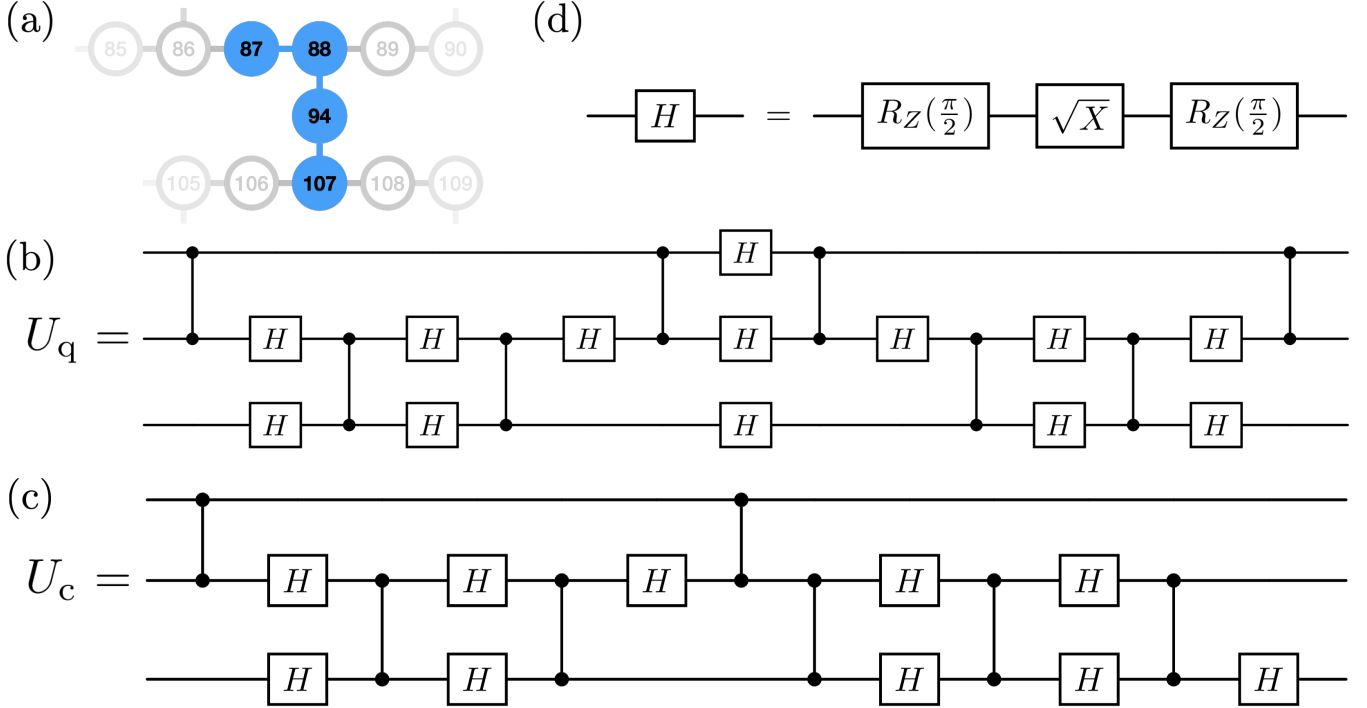


FIG. 6. Topology of the IBM Quantum processor (*ibm\_torino*) and circuit decompositions used. (a) Topology of the *ibm\_torino* where the blue solid circles are the qubits used to conduct the experiment. (b) Circuit decomposition of the Clifford quantum information scrambler  $U_q$  for *ibm\_torino*. (c) Circuit decomposition of the Clifford classical information scrambler  $U_c$  for *ibm\_torino*. (d) The circuit decomposition of each Hadamard gate  $H$  is given by a single  $\sqrt{X}$  gate and two  $R_Z$  (rotation around the  $Z$ -axis) gates with the rotational angle  $\pi/2$ .

- [26] Y. Sekino and L. Susskind, Fast scramblers, *J. High Energy Phys.* **2008**, 065 (2008).
- [27] N. Lashkari, D. Stanford, M. Hastings, T. Osborne, and P. Hayden, Towards the fast scrambling conjecture, *J. High Energy Phys.* **2013**, 22 (2013).
- [28] S. H. Shenker and D. Stanford, Black holes and the butterfly effect, *J. High Energy Phys.* **2014**, 67 (2014).
- [29] D. A. Roberts and D. Stanford, Diagnosing chaos using four-point functions in two-dimensional conformal field theory, *Phys. Rev. Lett.* **115**, 131603 (2015).
- [30] M. Blake, Universal charge diffusion and the butterfly effect in holographic theories, *Phys. Rev. Lett.* **117**, 091601 (2016).
- [31] P. Gao, D. L. Jafferis, and A. C. Wall, Traversable wormholes via a double trace deformation, *J. High Energy Phys.* **2017**, 151 (2017).
- [32] J. Maldacena, D. Stanford, and Z. Yang, Diving into traversable wormholes, *Fortschr. Phys.* **65**, 1700034 (2017).
- [33] B. Chen, B. Czech, and Z.-Z. Wang, Quantum information in holographic duality, *Rep. Prog. Phys.* **85**, 046001 (2022).
- [34] J. Liu, Scrambling and decoding the charged quantum information, *Phys. Rev. Res.* **2**, 043164 (2020).
- [35] E. Rinaldi, X. Han, M. Hassan, Y. Feng, F. Nori, M. McGuigan, and M. Hanada, Matrix-Model Simulations Using Quantum Computing, Deep Learning, and Lattice Monte Carlo, *PRX Quantum* **3**, 010324 (2022).
- [36] Y. Li, X. Li, and J. Jin, Information scrambling in a collision model, *Phys. Rev. A* **101**, 042324 (2020).
- [37] Y. Li, X. Li, and J. Jin, Dissipation-Induced Information Scrambling in a Collision Model, *Entropy* **24**, 345 (2022).
- [38] F. Tian, J. Zou, H. Li, L. Han, and B. Shao, Relationship between Information Scrambling and Quantum Darwin-

- ism, *Entropy* **26**, 19 (2024).
- [39] H. Shen, P. Zhang, Y.-Z. You, and H. Zhai, Information Scrambling in Quantum Neural Networks, *Phys. Rev. Lett.* **124**, 200504 (2020).
- [40] S. Choi, Y. Bao, X.-L. Qi, and E. Altman, Quantum Error Correction in Scrambling Dynamics and Measurement-Induced Phase Transition, *Phys. Rev. Lett.* **125**, 030505 (2020).
- [41] Z. Li, H. Zheng, Y. Wang, L. Jiang, Z.-W. Liu, and J. Liu, SU(d)-Symmetric random unitaries: Quantum scrambling, error correction, and machine learning, [arXiv:2309.16556](https://arxiv.org/abs/2309.16556) (2023).
- [42] B. Yan and N. A. Sinitsyn, Recovery of Damaged Information and the Out-of-Time-Ordered Correlators, *Phys. Rev. Lett.* **125**, 040605 (2020).
- [43] B. Yoshida and A. Kitaev, Efficient decoding for the Hayden-Preskill protocol, [arXiv:1710.03363](https://arxiv.org/abs/1710.03363) (2017).
- [44] B. Yoshida and N. Y. Yao, Disentangling Scrambling and Decoherence via Quantum Teleportation, *Phys. Rev. X* **9**, 011006 (2019).
- [45] N. Bao and Y. Kikuchi, Hayden-Preskill decoding from noisy Hawking radiation, *J. High Energy Phys.* **2021**, 17 (2021).
- [46] T. Schuster, B. Kobrin, P. Gao, I. Cong, E. T. Khabiboulline, N. M. Linke, M. D. Lukin, C. Monroe, B. Yoshida, and N. Y. Yao, Many-Body Quantum Teleportation via Operator Spreading in the Traversable Wormhole Protocol, *Phys. Rev. X* **12**, 031013 (2022).
- [47] K. A. Landsman, C. Figgatt, T. Schuster, N. M. Linke, B. Yoshida, N. Y. Yao, and C. Monroe, Verified quantum information scrambling, *Nature (London)* **567**, 61 (2019).
- [48] M. S. Blok, V. V. Ramasesh, T. Schuster, K. O'Brien, J. M. Kreikebaum, D. Dahlen, A. Morvan, B. Yoshida, N. Y. Yao, and I. Siddiqi, Quantum Information Scrambling on a Superconducting Qutrit Processor, *Phys. Rev. X* **11**, 021010 (2021).
- [49] J.-H. Wang *et al.*, Information scrambling dynamics in a fully controllable quantum simulator, *Phys. Rev. Res.* **4**, 043141 (2022).
- [50] I. Shapoval, V. P. Su, W. de Jong, M. Urbanek, and B. Swingle, Towards Quantum Gravity in the Lab on Quantum Processors, *Quantum* **7**, 1138 (2023).
- [51] G. Svetlichny, Time Travel: Deutsch vs. Teleportation, *Int. J. Theor. Phys.* **50**, 3903 (2011).
- [52] S. Lloyd, L. Maccone, R. Garcia-Patron, V. Giovannetti, Y. Shikano, S. Pirandola, L. A. Rozema, A. Darabi, Y. Soudagar, L. K. Shalm, and A. M. Steinberg, Closed timelike curves via postselection: Theory and experimental test of consistency, *Phys. Rev. Lett.* **106**, 040403 (2011).
- [53] S. Lloyd, L. Maccone, R. Garcia-Patron, V. Giovannetti, and Y. Shikano, Quantum mechanics of time travel through post-selected teleportation, *Phys. Rev. D* **84**, 025007 (2011).
- [54] W. J. van Stockum, The gravitational field of a distribution of particles rotating about an axis of symmetry, *Proc. R. Soc. Edinb.* **57**, 135–154 (1938).
- [55] K. Gödel, An example of a new type of cosmological solutions of Einstein's field equations of gravitation, *Rev. Mod. Phys.* **21**, 447 (1949).
- [56] M. S. Morris, K. S. Thorne, and U. Yurtsever, Wormholes, time machines, and the weak energy condition, *Phys. Rev. Lett.* **61**, 1446 (1988).
- [57] J. Friedman, M. S. Morris, I. D. Novikov, F. Echeverria, G. Klinkhammer, K. S. Thorne, and U. Yurtsever, Cauchy problem in spacetimes with closed timelike curves, *Phys. Rev. D* **42**, 1915 (1990).
- [58] J. R. Gott, Closed timelike curves produced by pairs of moving cosmic strings: Exact solutions, *Phys. Rev. Lett.* **66**, 1126 (1991).
- [59] D. Deutsch, Quantum mechanics near closed timelike lines, *Phys. Rev. D* **44**, 3197 (1991).
- [60] S. Deser, R. Jackiw, and G. 't Hooft, Physical cosmic strings do not generate closed timelike curves, *Phys. Rev. Lett.* **68**, 267 (1992).
- [61] S. W. Hawking, Chronology protection conjecture, *Phys. Rev. D* **46**, 603 (1992).
- [62] S. M. Carroll, E. Farhi, A. H. Guth, and K. D. Olum, Energy-momentum restrictions on the creation of Gott time machines, *Phys. Rev. D* **50**, 6190 (1994).
- [63] H. Monroe, Are causality violations undesirable?, *Found. Phys.* **38**, 1065–1069 (2008).
- [64] A. V. Shepelin, A. M. Rostom, V. A. Tomilin, and L. V. Il'ichov, Multiworld motives by closed time-like curves, *J. Phys. Conf. Ser.* **2081**, 012029 (2021).
- [65] S. Lloyd and J. Preskill, Unitarity of black hole evaporation in final-state projection models, *J. High Energy Phys.* **2014**, 126 (2014).
- [66] P. Xu *et al.*, Satellite testing of a gravitationally induced quantum decoherence model, *Science* **366**, 132–135 (2019).
- [67] I. H. Kim and J. Preskill, Complementarity and the unitarity of the black hole s-matrix, *J. High Energy Phys.* **2023**, 233 (2023).
- [68] O. Oreshkov and N. J. Cerf, Operational formulation of time reversal in quantum theory, *Nat. Phys.* **11**, 853–858 (2015).
- [69] S. M. Korotaev and E. O. Kiktenko, Quantum causality in closed timelike curves, *Phys. Scr.* **90**, 085101 (2015).
- [70] G. Chiribella and Z. Liu, Quantum operations with indefinite time direction, *Commun. Phys.* **5**, 190 (2022).
- [71] E. O. Kiktenko, Exploring postselection-induced quantum phenomena with time-bidirectional state formalism, *Phys. Rev. A* **107**, 032419 (2023).
- [72] D. R. M. Arvidsson-Shukur, A. G. McConnell, and N. Yunger Halpern, Nonclassical advantage in metrology established via quantum simulations of hypothetical closed timelike curves, *Phys. Rev. Lett.* **131**, 150202 (2023).
- [73] X. Song, F. Salvati, C. Gaikwad, N. Yunger Halpern, D. R. M. Arvidsson-Shukur, and K. Murch, Agnostic phase estimation, *Phys. Rev. Lett.* **132**, 260801 (2024).
- [74] Quantinuum H1-1, <https://www.quantinuum.com/>, (2024).
- [75] IBM Quantum, <https://quantum.ibm.com/>, (2021).
- [76] A. Javadi-Abhari *et al.*, Quantum computing with Qiskit, [arXiv:2405.08810](https://arxiv.org/abs/2405.08810) (2024).
- [77] M. A. Nielsen and I. L. Chuang, *Quantum Computation and Quantum Information: 10th Anniversary Edition* (Cambridge University Press, 2012).
- [78] M. Pawłowski, T. Paterek, D. Kaszlikowski, V. Scarani, A. Winter, and M. Żukowski, Information causality as a physical principle, *Nature* **461**, 1101 (2009).
- [79] D. A. Roberts and B. Yoshida, Chaos and complexity by design, *J. High Energy Phys.* **2017**, 121 (2017).